Magnetization temperature dependence and freezing of surface spins in magnetic fluids based on ferrite nanoparticles

R. Aquino* and J. Depeyrot
Complex Fluid Group, Instituto de Fisica, Universidade de Brasilia, Caixa Postal 04455, 70919-970 Brasilia (Distrito Federal), Brazil

M. H Sousa† and F. A. Tourinho
Complex Fluid Group, Instituto de Quimica, Universidade de Brasilia, Caixa Postal 04478, 70919-970 Brasilia (Distrito Federal), Brazil

E. Dubois and R. Perzynski
Laboratoire des Liquides Ioniques et Interfaces Chargees, Universite Pierre et Marie Curie, Bâtiment F, Case 63, 4 place Jussieu, 75252 Paris Cedex 05, France

(Received 15 September 2005; revised manuscript received 6 October 2005; published 30 November 2005)

Manganese and copper ferrite nanoparticles, in the size range 3.3–10.4 nm, are prepared by a hydrothermal coprecipitation process and peptized in aqueous solution. The thermal dependence of the high field magnetization is investigated in the dilute regime and the observed properties can be attributed to individual particles. Our results show that, at low temperatures, the structure of our nanoparticles can be seen as being made of a monodomain ordered core and a surface shell of disordered spins, which can fluctuate freely at high temperatures. Finite sizes effects have implications on the temperature dependence of the saturation magnetization m_S. Its variations are well accounted for by an effective Bloch law with an exponent larger than the bulk value for very small mean diameter (3.5 nm) and a Bloch constant slightly size decreasing for larger ones. A sharp increase of the high field magnetization, more marked as the size decreases, is evidenced at low temperature. It is related to a freezing of surface spins in a disordered state below a temperature of the order of 70 K and adjusted to a reduced exponential behavior.

DOI: 10.1103/PhysRevB.72.184435 PACS number(s): 75.50.Mm

I. INTRODUCTION

Interest in magnetic properties of nanosized ferrite particles is driven by both technological applications and theoretical researches.[1,2] If individually dispersed in a liquid carrier at room temperature, those nanoparticles lead to magnetic liquids. They are widely used in technological devices such as sensors of acceleration, tilting angle or pressure, in assisted shock absorbers or as magneto-optical modulators.[3,4] If dispersed in a complex medium like a clay, a liquid crystal, or a biological cell, they can be used as nanoscaled magnetic probes in order to investigate the local rheological properties of the carrier medium.[5] They also may be used to build new magnetoresponsive complex media such as magnetic gels[6] or magnetic vesicles, the magnetic nanoparticles being for example inserted inside a *d*-block polymeric membrane.[7] If dispersed in a solid matrix,[8] their applications essentially lie in their use in ultrahigh density magnetic information storage.[1] In biology, they are currently used as a magnetic resonance imaging (MRI) contrast agent.[9,10] Indeed, in all these applications, the static and dynamic magnetic behavior of the dispersed nanopaticles is of paramount importance.

From a more fundamental point of view, the reduction of the particle size at nanoscale raises up basic questions in magnetism. The particle magnetization cannot be seen as uniform through the nanomaterial. It is very probably the result of a magnetic ordered core and of a surrounding surface shell of disordered spins.[1,11] In a dilute dispersion of nanoparticles, it leads to a complex interplay between two kinds of phenomena: finite-size and interface effects. They are both enhanced as the particle size decreases since the surface to volume ratio becomes larger. They are both responsible for the thermal evolution of the nanoparticles magnetization.

Finite-size effects of the magnetic core are related to the low number of spins linked together in a cooperative behavior inside the core of the nanoparticle.[1,2] In a bulk ordered magnetic system and for temperatures enough below the Curie temperature (here of the order of 700 K), the temperature dependence of the magnetization is driven by spin-wave excitations. It leads to the well-known Bloch $T^{3/2}$ law when the gap resulting from crystalline anisotropy and/or demagnetizing field is zero. However, at the nanoscale, significant deviations to this law have been predicted calculating the spin-wave spectra of spherical Heisenberg spin clusters.[12] Due to their finite size, an effective law, function of T^{α}, can be deduced. The exponent α is size dependent, larger than the bulk value 3/2 and found to be of the order of 2 for nanosized iron particles of 2.0 nm and also for magnetite based ferrofluids.[13,14] Experimental determinations, available to confirm this nanomagnetic prediction, are rather scarce.[15,16]

Interface (or surface) effects are related to the lack of coordination for the surface ions. It does induce a large number of broken exchange bonds for surface atoms, which can, therefore, result in frustration and spin disorder. In zero field and high temperatures (typically $T \geqslant 100$ K for γ-Fe_2O_3 nanoparticles), those surface spins fluctuate. To our knowledge,[2] the only direct experimental evidence of this dynamical behavior up to now has been performed by inelas-

tic neutron scattering.[17] On the contrary, at low temperature ($T<100$ K), the spin disorder is frozen and more easy to detect.[18,19] Indeed, for magnetic fields as large as a few 10^2-10^3 kA/m, which are much larger than the anisotropy field of the nanoparticle core,[1] nonsaturated hysteresis loops are sometimes observed, for example, for maghemite[18] and for nickel ferrite[19] nanoparticles. Moreover, a magnetization much smaller than that of the bulk saturation magnetization is frequently measured.[19] Such observations have been attributed to the existence of surface canted spins.[20] This canting is also detected by Mossbauer spectroscopy performed under a field parallel to the direction of the incident γ rays through the observation of an incomplete polarized spectrum.[20,21] Besides this, an additional contribution, usually also attributed to the canted surface spins, modifies the magnetization temperature dependence at low temperature.[22] As an example, for ultrasmall γ-Fe_2O_3 particles, at temperatures typically lower than 100 K, the thermal variation of magnetization displays a steep rise, more and more pronounced as the particle size decreases.[23] A similar behavior is observed in amorphous ferromagnetic nanoparticles.[24] If often observed, this steep rise of magnetization at low temperatures is still a theoretical open question which has never been systematically studied experimentally. A study as a function of the size of the nanoparticles in well-defined systems would help to understand those surface effects by tuning the surface-to-volume ratio in controlled conditions.

We are currently working on the synthesis of individual nanoparticles of ferrite via a soft chemical bottom-up route.[25,26] Experts in the dispersion in aqueous media standardly test it by small angle neutron scattering.[26–28] Via a thermodynamical size sorting at room temperature based on a well-established phase diagram,[27] we are able to reduce the size polydispersity of the nanoparticles and to tune their mean diameter in aqueous solutions.[29] Thanks to this process, we have been able to accurately evidence, in our γ-Fe_2O_3 nanoparticle dispersions, the size dependencies of ferromagnetic resonance spectra.[29] Those experiments have demonstrated the dominating surface origin of the anisotropy field in those nanoparticles.[11,29] Moreover, in high fields, and at low T, the freezing of the badly correlated surface spins leads to an additional unidirectional anisotropy field, as it is observed with systems presenting a standard spin glass behavior in low fields.[30]

Following the same experimental procedure as in Ref. 29, we propose here to investigate in detail the thermal and nanoparticle size dependences of the high field magnetization of colloidal dispersions of ferrite nanoparticles. The small size of the nanoparticles indeed leads to enhanced finite-size and surface spins effects. However, it is essential to have nanoparticles all obtained in a well-defined and comparable way in order to evidence the size dependencies of these properties. We use manganese and copper ferrite nanoparticles with a mean diameter ranging from 3.3 nm to 10.4 nm with a relative standard deviation ranging between 15% and 30%. We explore the dilute regime of concentration where, at $T=300$ K, the interparticle repulsion leads to a system of individually dispersed nanoparticles. As it has been previously verified in Refs. 17 and 29, such a quickly quenched system keeps its dispersed organization at low temperatures. We analyze the thermal variations of magnetization in high fields in terms of a modified Bloch law, accounting for both finite-size effect and an extra surface contribution below $T=70$ K. It indeed confirms that one should distinguish in the magnetic nanostructures of the particles the single-domain core from the surface spins, which can fluctuate freely at high temperatures.

II. EXPERIMENTAL DETAILS AND CHARACTERIZATION

A. Particle synthesis and magnetic fluid elaboration

The magnetic fluid (MF) preparation is carried out in three basic steps:[25] (i) the ferrite nanoparticle synthesis, (ii) the chemical surface treatment, and (iii) the peptization of the particles in a stable aqueous colloidal solution. Ferrite nanoparticles are prepared using a hydrothermal coprecipitating aqueous solution of a MCl_2-$FeCl_3$ (M=Mn or Cu) mixture in alkaline medium.[31] After the coprecipitation step, the precipitate is washed in order to reduce the high ionic strength of the medium and the particle surface is cleaned by a (2 mol L^{-1}) HNO_3 solution. Moreover, to ensure the thermodynamical stability of the particles, an empirical process is used: the precipitates are boiled with a 0.5 mol L^{-1} of $Fe(NO_3)_3$ solution. Then, the particles are conveniently peptized in an acidic medium by the adjustment of the ionic strength, resulting in a stable solution. We obtain samples with different nanoparticle mean diameters using various procedures. In the case of manganese ferrite samples, the nanoparticle size has been controlled during the ferrofluid synthesis by the hydroxide concentration.[32] For copper ferrite nanoparticles, a colloidal size sorting process[29] leads to samples with different mean diameters and very low polydispersity.

B. Characterization of the synthesized dispersions

The structure, morphology, and mean diameter of our nanoparticles are determined through x-ray powder diffractogram and TEM pictures.[31,32] Table I lists the size characteristics of the samples and allows us to compare the results obtained by x-ray diffraction with those determined by electron microscopy. Indeed, the crystalline size d_{XR} well match a lognormal size distribution by using the relation $d_{XR}=d_0e^{2.5S_d^2}$, where d_0 (defined as $\ln d_0=\langle \ln d\rangle$) and S_d the standard deviation of $\ln d$ are determined from the TEM histogram analysis.[33] Furthermore, these data show the efficiency of the size sorting process, since the standard deviation S_d determined for Cu-based samples typically stands between 0.15 and 0.18, values much smaller than those obtained for Mn-based samples. In order to determine the samples compositions, suitable chemical titrations are performed for all MF samples based on $CuFe_2O_4$, and $MnFe_2O_4$ ferrites. Iron (III) titration is performed by dichromatometry and copper (II) titration by volumetric analysis with iodine. The manganese (II) concentration is determined using inductively coupled plasma atomic emission spectroscopy (ICP-AES). Table II lists the volume fraction in magnetic nanomaterial (ϕ) for all samples.

TABLE I. Sample characteristics: d_{XR} is the mean diameter deduced from x-ray powder diffractogram, d_0 is the characteristic size obtained from TEM pictures, and S_d is the standard deviation of $\ln(d)$.

Sample[a]	d_{XR}(nm)[b]	d_0(nm)[b]	S_d[b]
Mn1	9.0	8.0	0.25
Mn2	7.4	6.4	0.27
Mn3	4.2	3.3	0.3
Mn4	3.3	2.8	0.3
Cu1	10.4	9.6	0.18
Cu2	7.5	7.0	0.16
Cu3	6.3	5.9	0.15
Cu4	3.5	3.2	0.17

[a]Mn samples based on $MnFe_2O_4$ and Cu samples based on $CuFe_2O_4$.
[b]Uncertainties of the order of 10%.

C. Magnetic measurements

The superconducting-quantum-interference-device (SQUID) magnetometer from Groupe de Physique de Solide–Université Pierre et Marie Curie–France is used to perform magnetic measurements for all MF samples between 5 K and 300 K. The temperature dependence of the saturation magnetization $M_S(T)$ is obtained from two different zero field cooled measurements: (i) hysteresis loops recorded at various temperatures in a magnetic field (H) range -4×10^3 kA/m$<H<4\times10^3$ kA/m and (ii) direct measurements of $M_S(T)$ at $H=4\times10^3$ kA/m. In our experiments, the carrier medium is aqueous so that below 273 K, it becomes solid. If the freezing process is sufficiently rapid, the magnetic solution maintains the same state of particle dispersion than at room temperature. Small angle neutron scattering experiments performed at 300 K and freeze fracture TEM pictures[27] show that in our concentration range and conditions of pH and of ionic strength the interparticle interaction is negligible.[26] Our experimental system is, therefore, constituted by individual nanoparticles dispersed in a solid matrix.

D. Magnetic moment distribution

At 300 K and for enough dilute solutions (for a dipolar interaction parameter smaller than 1 at 300 K, thus typically here for volume fractions ϕ smaller than a few percent),[28] the magnetic fluid response to an applied field H results from the progressive orientation in the field of an ensemble of noninteracting magnetic moments, which are free to rotate in the solvent. This giant paramagnetic behavior is well described by the Langevin formalism taking into account a lognormal distribution of magnetic moments $\mu=m_SV$, m_S being the magnetization of the nanomaterial, V the magnetic volume of the nanoparticles

$$Q(\mu)=\frac{1}{\mu S_\mu\sqrt{2\pi}}\exp\left[-\frac{\ln^2(\mu/\mu^0)}{2S_\mu^2}\right], \tag{1}$$

S_μ is the polydispersity index of $\ln\mu$ and $\ln\mu^0=\langle\ln\mu\rangle$ (by definition $S_\mu=3S_d$). Then, the magnetization of the colloidal solution is a superposition of the contribution of each particle weighted by the distribution of magnetic moments. It writes

$$\frac{M}{m_S\phi}=\frac{\int L[\xi(\mu,S_\mu)]Q(\mu)d\mu}{\int Q(\mu)d\mu}, \tag{2}$$

where $\xi=\mu_0\mu H/k_BT$ and $L(\xi)=\coth\xi-1/\xi$ are, respectively, the Langevin parameter and the Langevin function,[3] μ_0 be-

TABLE II. Sample characteristics: ϕ is the volume fraction of nanoparticle, $\langle\mu\rangle$ is the mean magnetic moment of the nanoparticles at 300 K and S_μ the polydispersity index of $\ln\mu$, both deduced from magnetization measurements [see Fig. 1 and Eq. (2)], m_S is the magnetization of the nanomaterial at $T=300$ K and $H=4\times10^3$ kA/m, $\langle\xi\rangle=\mu_0\langle\mu\rangle H/k_BT$ then corresponds to the mean Langevin parameter calculated in those T and H conditions.

Sample[a]	Symbol	ϕ (%)	$\langle\mu\rangle$[b] ($10^3\ \mu_B$)	S_μ	m_S(300 K)[c] (kA/m)	$\langle\xi\rangle$[d]
Mn1	▽	0.45	17.2	1.20	375	194
Mn2	◯	1.54	6.5	1.30	285	73
Mn3	□	0.45	3.3	1.40	250	37
Mn4	△	0.45	1.1	1.20	130	12
Cu1	⊕	2.28	16	0.93	172	193
Cu2	⊞	1.32	4.2	1.15	113	44
Cu3	*	1.39	3.8	1.15	105	21
Cu4	◇	1.77	0.6	1.30	92	6.9

[a]Mn samples based on $MnFe_2O_4$ and Cu samples based on $CuFe_2O_4$.
[b]Error of $R^2=0.999$.
[c]Uncertainties of the order of 5%.
[d]300 K, 4×10^3 kA/m).

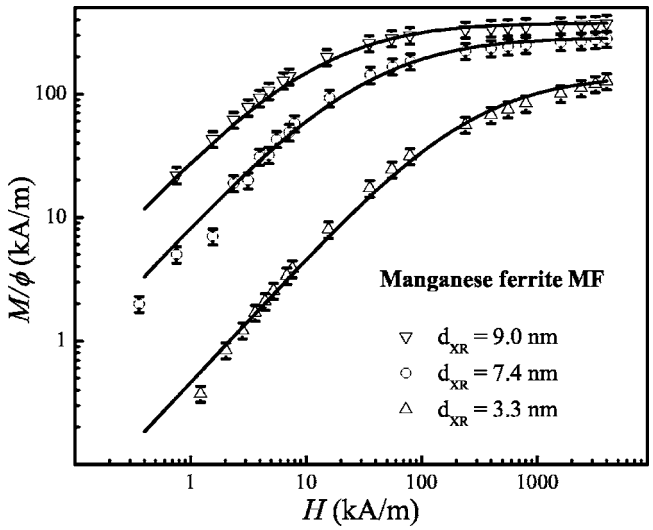

FIG. 1. Room temperature magnetization for manganese ferrite based MF (▽: Mn1, O: Mn2, △: Mn4). The full lines are the best fits obtained using Eq. (2) and the parameters of Table II. For sample characteristics, see Tables I and II.

ing the permeability of the vacuum and k_B the Boltzmann constant.

III. RESULTS

A. Room temperature measurements

As an example, Fig. 1 displays the experimental magnetization curves of $MnFe_2O_4$ samples of various diameters (Mn1, Mn2, and Mn4). The best fits are obtained using Eq. (2). Table II gives also the values of the mean magnetic moment $\langle\mu\rangle$, the polydispersity S_μ deduced from the best fit, and the mean Langevin parameter $\langle\xi\rangle$ calculated at 300 K and 4×10^3 kA/m. Note in Fig. 1 that the magnetization of sample Mn4(d_{XR}=3.3 nm) is not fully saturated at a field as large as 4×10^3 kA/m.

B. Low temperatures measurements

Figure 2 shows typical hysteresis loops measured at various temperatures for manganese ferrite based samples Mn2 [Figs. 2(a) and 2(b); d_{XR}=7.4 nm] and Mn4 [Figs. 2(c) and 2(d); d_{XR}=3.3 nm]. A similar behavior is observed for all our

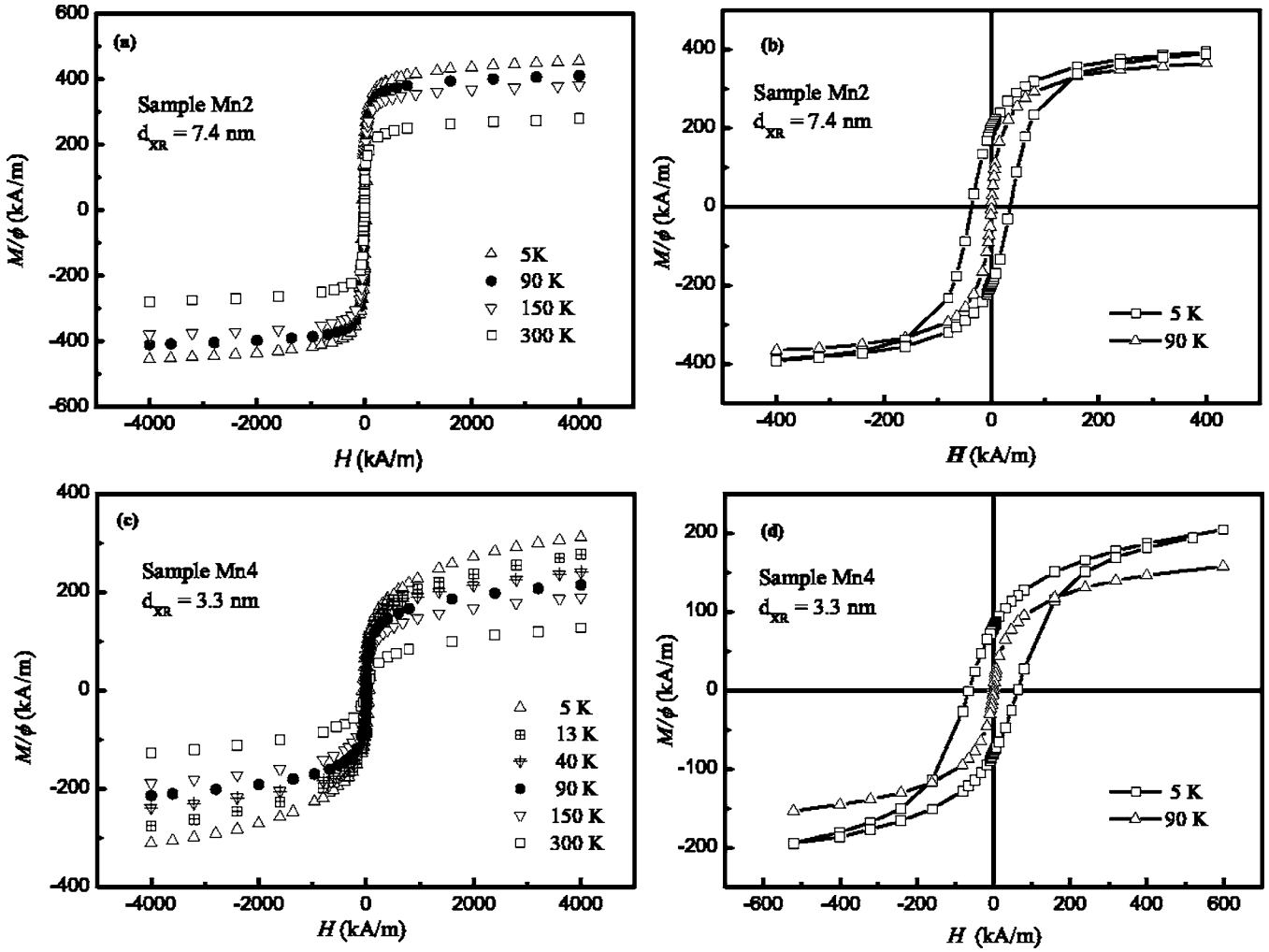

FIG. 2. (a) and (c): hysteresis loops recorded at various temperatures for samples Mn2 and Mn4, respectively. (b) and (d): opened loops at 5 K and closed ones at 90 K.

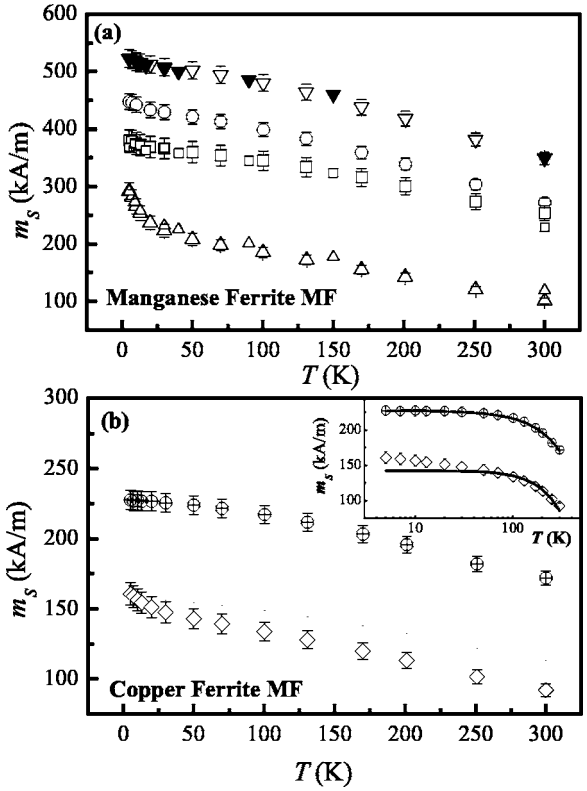

FIG. 3. (a) and (b) display the temperature dependence of the magnetization m_S. The inset of (b) compares in a semilogarithmic plot the m_S determination of samples Cu1 and Cu4 and their core saturation (full line). For symbols, see Table II.

MFs. For samples based on the largest particles, the magnetization curves experimentally reach the saturation in high fields at 300 K (see Fig. 1). However, for samples based on the smallest ones, the magnetization does not saturate (see Fig. 2), the nonsaturation behavior being more pronounced as the temperature decreases. Figures 2(b) and 2(d) represent the details of the corresponding loops at 5 K (opened loop) and 90 K (closed loop). The experiments are zero field cooled and we only observe symmetric loops. They are associated at 5 K to coercive field 36.8 kA/m (Mn2; d_{XR} =7.4 nm) and 64.0 kA/m (Mn4; d_{XR}=3.3 nm). At a temperature of 90 K, the irreversibility no longer exists showing, therefore, that, for both samples, the coercive field vanishes rapidly with increasing temperature.

We call m_S the magnetization measured at 4×10^3 kA/m and normalized by the volume fraction in magnetic material. Figures 3(a) and 3(b) display the temperature dependence of m_S for manganese-based and copper-based magnetic fluids, respectively. In Fig. 3(a), we compare, for sample Mn1, the direct measurements (open symbols) of $m_S(T)$ to the values of m_S obtained from the hysteresis loops (solid symbols) recorded at various temperatures. As it can be seen, both determinations well overlap. Figures 3(a) and 3(b) exhibit a smooth increase of m_S as T is decreasing, associated to a steeper behavior at the lowest temperatures (typically below 50 to 100 K), which is very pronounced for the smallest particles. This steeper behavior can be assigned to the surface spins contribution.[22–24] In the following, we shall distinguish two extreme regimes: (i) *"large particles, high temperatures,"* which can be described by an effective Bloch formalism, (ii) *"small particles, low temperatures,"* and where an additional surface contribution, the larger for the smaller particles, has to be taken in account.

IV. DISCUSSION

We discuss here our results, in the framework of a core-shell model, taking into account both the finite-size effects in an effective Bloch formalism and the thermal dependence of the disordered surface contribution.

A. Finite-size effects and effective bloch law

The thermal behavior of the magnetization of ordered magnetic systems is due to low energy collective excitations, well known as spin waves or magnons, and results in a decrease in the spontaneous magnetization with increasing temperature. Such a model, which leads to the Bloch $T^{3/2}$ law well works for infinite systems if the gap, induced in the dispersion relation of spin waves, is zero.[2] Nevertheless, the behavior for small clusters and nanoparticles is different from that of bulk materials since the spatial confinement reduces the number of degrees of freedom. It generates an energy gap in the corresponding spin-wave spectrum.[13] As a result of the existence of this energy gap in the density of states for the spin waves, added to the lowering of the mean number of nearest neighbors, the temperature dependence of the magnetization of the cores of the nanoparticles can be well described with a more general law[21,34]

$$m_S(T) = m_S(0)(1 - BT^{\alpha}), \tag{3}$$

where $m_S(0)$ is the saturation magnetization as T tends to zero. Note that experimentally $m_S(0)$ has to be extrapolated, getting rid of the additional surface contribution at low temperatures. The exponent α is now size dependent and structure independent, whereas the Bloch constant B mainly depends on the detailed structure of the core of the nanoparticles. If this modified Bloch's law holds, a double logarithmic plot of the depression of the core magnetization $m_S(0)-m_S(T)$ as a function of T should give straight lines of respective slopes α.[15]

However, it is important to note that this model would work only if the applied field is large enough to ensure the saturation condition for the core of the nanoparticles in each sample. In other words, in the whole temperature range the magnetic energy must be much larger than the anisotropy energy and the thermal energy (meaning a Langevin parameter $\langle\xi\rangle \gg 10$).

As it can be seen in Fig. 2, the closure field is always much smaller than the maximum field used in our experiments so that the first condition is always satisfied. On the contrary, it is clear that the second condition is not fulfilled (see Table II) at T=300 K and $H=4\times10^3$ kA/m for samples labeled Mn4 and Cu4 (the samples of smallest mean diameters). In order to compensate the nonsaturation for those samples, a correction is made replacing in Eq. (3) $m_S(T)$ by $m_S(T)/\{L[\xi(T)]\}$ where $\xi(T)$ is calculated at each tempera-

TABLE III. $m_S(0)$: saturation magnetization of the nanoparticle core extrapolated at $T=0$; α: the temperature exponent obtained from a fit of $m_S(0)-m_S(T)$ to Eq. (3), α and B being free parameters; B: Bloch constant calculated for our samples using Eq. (3) with $\alpha=3/2$; B_{bulk}: Bloch constant of the bulk material from Ref. 26. A_{surf}(5 K): value of the surface contribution A_{surf}(5 K) from Eq. (4) taken at 5 K.

Sample	$m_S(0)$ (kA/m)	α	B	B_{bulk} (10^{-5} K$^{-3/2}$)	A_{Surf}(5 K) (10^{-5} K$^{-3/2}$)
Mn1	515	1.45±0.02	6.46±0.13		0.020
Mn2	430	1.60±0.03	7.10±0.14	6.33	0.043
Mn3	366	1.64±0.01	6.60±0.13		0.040
Mn4	200	2.03±0.12			0.462
Cu1	228	1.40±0.03	4.81±0.09		<0.005
Cu2	157	1.59±0.03	5.00±0.10	3.46	0.012
Cu3	144	1.44±0.03	5.70±0.12		0.023
Cu4	148	2.01±0.15			0.088

ture, by using the value of the mean magnetic moment $\langle\mu\rangle$ of Table II. This small correction being taken into account, the high temperature variations of $m_S(T)$, which are associated to the regular saturation of the grain core, are fitted with Eq. (3). This adjustment leads to $m_S(0)$, the extrapolated values of m_S for the grain core at $T=0$ [see Table III and Fig. 4(a)]. As an example, the inset of Fig. 3(b) shows two semilogarithmic representations of the experimental variation of $m_S(T)$ and their corresponging core saturation for copper ferrite MF (Cu1 and Cu4). For the largest particles, the whole range of temperature can be adjusted by Eq. (3); on the contrary, for the smallest ones, the extra surface contribution appears clearly below roughly 70 K. This also leads to the exponent α and the Bloch constant B (see Table III).

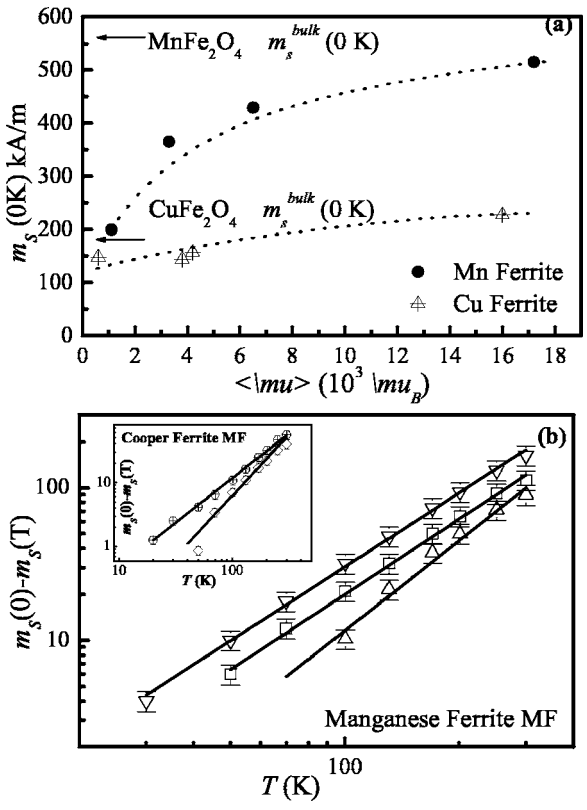

FIG. 4. (a) The core magnetization $m_S(0)$ extrapolated from experimental values as a function of the mean magnetic moment $\langle\mu\rangle$ of the nanoparticles. (b) Depression of the core magnetization $m_S(0)-m_S(T)$ for our samples in a double logarithmic representation. The full line corresponds to the best fit using Eq. (3) and yields the value of α. For symbols, see Table II.

Figure 4(a) plots the experimental extrapolated values of the core magnetic saturation $m_S(0)$ as a function of the mean magnetic moment $\langle\mu\rangle$ of the particles for each material. If for nanoparticles based on $MnFe_2O_4$, $m_S(0)$ is always smaller than the bulk value at $T=0$ (560 kA/m), it is not the case for $CuFe_2O_4$ [$m_S^{\text{bulk}}(T=0)=160$ kA/m]. Our copper ferrite nanoparticles, under field Mossbauer spectroscopy, have shown that the crystalline structure corresponds to a mixed spinel type in which the ratio of Fe^{3+} ions at octahedral sites and tetrahedral ones is indeed different from 1, the value expected for an ideal inverse spinel structure. It is found equal to 1.54 independently of the size of the nanoparticles.[35] This cation redistribution could, therefore, induce an increase on the $m_S(0)$ value.

The depression of the core magnetization $m_S(0)-m_S(T)$ is plotted for a few samples in Fig. 4(b) as a function of T. In that log-log representation, the variations are linear with a slope α. For samples of largest mean diameters, and both for copper and manganese ferrite nanoparticles, the values are found to be of the order of 1.5, in good agreement with the expected Bloch behavior for bulk materials. On the contrary, for the two samples based on the smallest nanoparticles, the straight lines clearly lead to larger slopes and are, therefore, associated to a deviation of the $T^{3/2}$ Bloch law with α approximately equal to 2 (see Table III). In that case, the fit with Eq. (3) is performed for $T \geqslant 70$ K. Indeed, the finite size strongly affects the exponent value only for the two samples based on the smallest nanoparticles of mean diameter around 3.5 nm.

Table III lists the values of B (Bloch constant) obtained when the $T^{3/2}$ law works and compares these values to those deduced for bulk materials from data of Ref. 26. (i) In the case of manganese ferrite nanoparticles, the B values are slightly larger, but close to that of the bulk. (ii) For samples

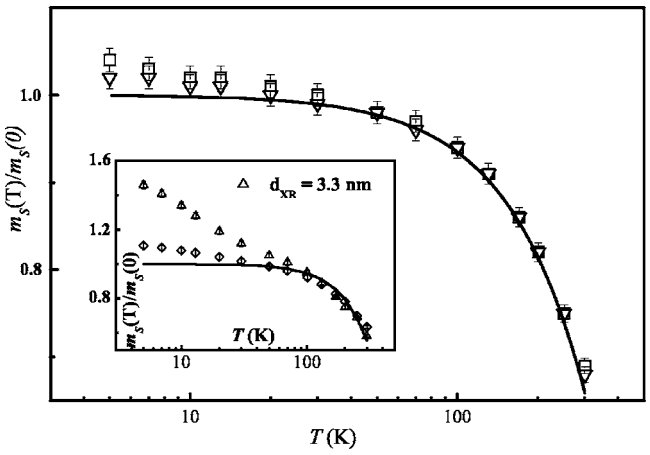

FIG. 5. Semilogarithmic plot of the experimental saturation magnetization normalized by the core value at $T=0$ K for samples Mn1 and Mn3. The full line is the fit using Eq. (3) with $\alpha=1.5$ and $B=6.46\times10^{-5}$ K$^{-3/2}$. The inset plots this variation for samples of smaller sizes of Mn4 and Cu4; the full line is the corresponding fit using Eq. (3) with $\alpha=2.0$. For symbols, see Table II.

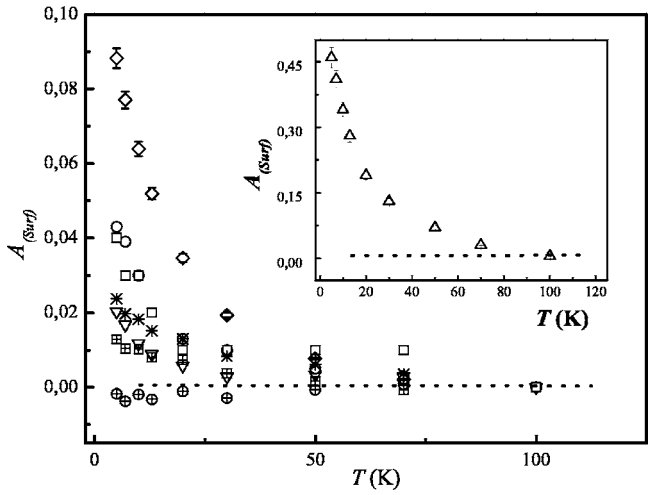

FIG. 6. Thermal variations of the surface contribution A_{surf}. The inset displays this variation for sample Mn4. For symbols, see Table II.

based on copper ferrite, the B values found are 40% larger than the corresponding bulk ones. This could be related to cation redistribution in interstitial sites of the ferrimagnetic core.[35]

For both manganese and copper ferrite nanoparticles, the constant B slightly increases as d_{XR} decreases. Let us assume that the cation distribution is constant with size for both kinds of ferrite nanoparticles. The observed size dependence of B then can be related to the existence of a rather important contribution in ferrite nanoparticles,[36] coming from surface canted spins poorly correlated to the monodomain core.[8,12] Indeed at the interface, the reduction of atomic coordination implies that surface spins are more sensitive to thermal fluctuations, which favors an effective B increasing.

B. Surface spins freezing

We analyze, in the following, the deviation to the effective Bloch law observed at low temperatures [see inset of Fig. 3(b)]. Indeed, for temperatures lower than approximately 70 K to 100 K, a sharp increase of the saturated magnetization, more pronounced with decreasing size, is experimentally observed. It is illustrated in the inset of Fig. 3(b) and in Fig. 5, which displays, in a semilogarithmic representation, the reduced variations of $m_S(T)/m_S(0)$. As an example, if this deviation is almost null for sample Cu1, it represents, at $T=5$ K, 10% of $m_S(0)$ for sample Cu4 and 46% for Mn4. Such low temperature deviations to the effective Bloch law have been already observed for ferrite nanoparticles.[37] They are usually addressed to misaligned surface spins. However, to analyze it, no definitive theoretical model is presently available. In metallic nanoparticles, this extra contribution is sometimes taken in account by introducing a temperature dependence of the Bloch constant as in itinerant magnets, for example.[38] Such an analysis is not adapted to ferrites. Moreover, for the smaller particles, the experimental observations cannot be seen as small deviations to the generalized Bloch law of Eq. (3) as it would require a negative Bloch constant! Those deviations being strongly temperature dependent, we propose to take into account those deviations by an additive surface contribution $A_{surf}(T)$ to Eq. (3) in the following form:

$$m_S(T)/m_S(0) = (1 - BT^{\alpha}) + A_{surf}(T). \tag{4}$$

Arbitrarily, this simple phenomenological description does not couple the temperature dependence of the core magnetization to that of the surface. It should be seen as a first step to describe the magnetization contribution of this badly known surface layer. Equation (4) should be able to retrieve the three following experimental points we establish here. Future rigorous theoretical models, which would restore the coupling between the magnetic core and the external shell, will have to recover these three points.

(i) The onset of an extra contribution to $m_S(T)$ roughly below 70 to 100 K: Figure 6 presents the thermal variations of the extra term $A_{surf}(T)$ for all our samples. One can easily see that $A_{surf}(T)$ is experimentally different from zero only for temperatures lower than say 70 to 100 K and for all our samples, except for sample Cu1 for which it appears null in the whole range of T. In this sample, the nanoparticles have the largest mean diameter and, therefore, the smallest surface-to-volume ratio. For Cu1, the contribution $A_{surf}(T)$ is found smaller than the accuracy of the measurement.

(ii) The dependence on the nanoparticle size of this extra contribution: The amplitude of the effect strongly depends on the nanoparticle diameter. Table III lists the experimental values of $A_{surf}(5\text{ K})$ for each sample, it increases as the nanoparticle diameter decreases, that is, as the surface-over-volume ratio increases.

(iii) Its strong temperature dependence: The thermal variations of the surface contribution are strongly temperature dependent and are going to zero at high temperatures. We thus propose an expression of the following form to approach the thermal variation of the surface term:

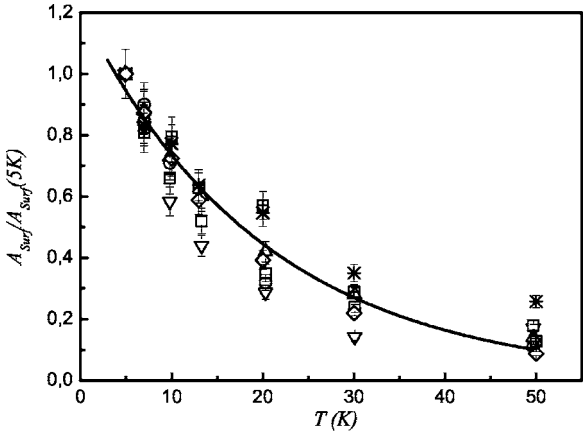

FIG. 7. Variations of $A_{surf}/A_{surf}(5\ \mathrm{K})$ as a function of T with $T_{freezing}=20$ K and $A=1.2A_{surf}(5\ \mathrm{K})$. The full line corresponds to Eq. (5) with $a=2.7$, the mean value of a in Table II. For symbols, see Table II.

$$A_{surf}(T) = A\exp(-T/T_{freezing}), \tag{5}$$

where A and $T_{freezing}$ are experimental parameters which are *a priori* material and nanoparticle size dependent. This phenomenological law is similar to that of electron paramagnetic resonance (EPR) linewidth in canonical bulk spin glasses, attributed either to a broadening from a distribution of internal local fields or to a slowing down of the spin-relaxation rate on approaching $T_{freezing}$.[39]

Here, whatever the material ($CuFe_2O_4$ or $MnFe_2O_4$) and the nanoparticle size of the dispersion (from 3 to 10 nm), the temperature $T_{freezing}$, obtained from the fit of the data to Eqs. (4) and (5), is roughly a constant and its mean value is

$$\langle T_{freezing}\rangle = 20 \pm 5\ \mathrm{K}. \tag{6}$$

The parameter, which is here nanoparticle dependent, is the coefficient A, which is found equal to

$$A = (1.2 \pm 0.1)A_{surf}(5\ \mathrm{K}). \tag{7}$$

Figure 7 shows the reduced variation of the ratio $A_{surf}/A_{surf}(5\ \mathrm{K})$ as a function of T for the whole set of investigated samples and its fit to Eq. (5). All the experimental points, obtained for samples presenting different polydispersities lie on the same master curve, showing, therefore, that the general behavior of the surface contribution does not seem to be strongly influenced by the size dispersion of our samples. The value obtained for $T_{freezing}$ perfectly explains why the surface contribution disappears above say 70–100 K. For a temperature of the order of $3T_{freezing}$ (that is 60 K), the exponential term is of the order of 5%, that is of the order of our accuracy on $A_{surf}(T)$. At $T=80$ K, the exponential term is of the order of 2%. Moreover, we obtain an energy $kT_{freezing}=(2.7\pm0.7)\times10^{-22}$ J, which is of the same order of magnitude as the superexchange coupling constant inside the nanomaterial (for example, in $MnFe_2O_4$ the antiferro coupling energy[40] $|J_{AB}|$ between first neighbors is 3.0×10^{-22} J).

As mentioned above, for low temperatures, such a steep rise of the magnetization has been already evidenced for ferrite nanoparticles, but never carefully followed as a function of the nanoparticle size. It has been attributed to misaligned surface spins due to broken exchange bonds. Those spins do fluctuate more freely at high temperatures than the ones from the core and freeze progressively at low temperatures in a disordered structure.[17,19,41] Such a progressive freezing of the disordered surface has already been observed in maghemite nanoparticles using ac susceptibilities measurements[41] or quasielastic neutron scattering.[17] It has been attributed to fluctuations of surface spins that become frozen, in zero and low field, in a "spin-glasslike" structure.[18,28,42] The thermal behavior of the surface contribution of our investigated nanoparticles which follows the exponential law of Eq. (6) could be related to a corresponding transition in large fields. The energy $kT_{freezing}$ is then intimately related to the superexchange interactions, which pin the interacting spins in the frozen disordered layer.

In this paper, we have tested the size and thermal dependences of the surface contribution to the high field magnetization at low temperatures. The experimental investigation is here driven at rather low polydispersity in nanoparticle size and similar synthesizing conditions. In the future, it would be interesting to check, tuning different synthesizing conditions, if it could be possible to enhance or reduce this magnetic surface disorder and its contribution to the high field magnetization.

Let us finally note that, in low fields, a glassy state, which is mainly due to interparticle interactions, has been observed in powder samples based on various kinds of nanoparticles.[36,41] We are dealing here with very dilute samples of completely opposite spatial organization. The exchange interparticle interaction is here negligible and the dipolar interparticle interaction, even if large at 5 K, is however very weak in front of $\mu_0\mu H$. This dipolar interparticle interaction, nevertheless, penalizes the possibility to observe a pure effect of surface freezing at low T on the field cooled (FC) low field susceptibility as in Ref. 18.

V. SUMMARY AND PERSPECTIVES

Using a soft chemical method, we successfully synthesize magnetic nanoparticles of controlled size, based on manganese and copper ferrite. Their temperature dependent magnetic behavior is here investigated as a function of the nanoparticle size in dilute magnetic fluids. The nanoparticles are here individually dispersed with a large interparticle distance (larger than four times the particle diameter). Magnetization measurements have shown that the magnetic properties at 300 K are well described by a single domain configuration; a simple Langevin model leading to the magnetic moments distribution.

At low temperatures, the explored thermodynamic properties are strongly affected by finite size and surface effects. (i) For both kinds of ferrite, magnetic fluid samples based on particles of smallest mean diameters (close to 3.5 nm) present a significant deviation from the Bloch $T^{3/2}$ law for the temperature dependence of the saturation magnetization. An effective exponent around 2 is found experimentally instead of 1.5. (ii) For all other samples, and typically for $T > 70$ K, the observed behavior is similar to that of bulk ma-

terials with a Bloch $T^{3/2}$ law and a Bloch constant slightly increasing as the nanoparticle size is decreasing. It could be due to the surface disorder. If in the case of manganese ferrite nanoparticles B is close to its bulk value, for copper-ferrite-based samples, the smallest Bloch constant is 40% larger than the bulk one. We ascribe it to a cation redistribution in the nanoparticle core evidenced by Mossbauer spectroscopy.

At temperatures lower than 70–100 K, an additional contribution to the high field magnetization is observed. It is ascribed to surface spins misaligned with those of the ordered core, which freezes in a disordered structure at lower temperatures. This extra contribution is more pronounced as the mean diameter decreases; it can reach 30% of the low temperature magnetization for nanoparticles of diameter of the order of 3 nm. The extra contribution also presents exponential variations as a function of T below roughly 70 K and for any sample is proportional to the $\exp(-T/T_{freezing})$, the energy $kT_{freezing} \approx 2.7 \pm 0.7 \times 10^{-22}$ J being of the order of the superexchange constant inside the nanoparticle material.

It would be interesting to extend the exploration of those high field finite-size and surface effects to individually dispersed nanoparticles of different structure, metallic ones, for example, and to other various controlled states of dispersion such as dilute aggregated solutions or concentrated dispersed solutions.

ACKNOWLEDGMENTS

The authors are greatly indebted to L. Legrand, from the Groupe de Physique de Solide of Universite Paris 6, who allowed us to perform our magnetization measurements using a SQUID magnetometer. They thank Professor Yuri L. Raikher for helpful discussions. This work was supported by the Brazilian and French agencies through the contracts of international cooperation CAPES/COFECUB No. 292/99 and CNPq/CNRS No. 14286. We also acknowledge the financial support of the Brazilian agencies CNPq, CAPES and FINATEC.

*Corresponding author. Also at LI2C—Universite Pierre et Marie Curi. Electronic address: reaquino@unb.br
†Also at LI2C—Universite Pierre et Marie Curie.

[1] X. Batlle and A. Labarta, J. Phys. D **35**, R15 (2002).
[2] R. H. Kodama, J. Magn. Magn. Mater. **200**, 359 (1999).
[3] B. Berkovsky, *Magnetic Fluids and Applications—Handbook* (Begell House, New York, 1996).
[4] R. Rosensweig, *Ferrohydrodynamics* (Cambridge University Press, Cambridge, 1985).
[5] Yu. L. Raikher, V. I. Stepanov, J-C. Bacri, and R. Perzynski, Phys. Rev. E **66**, 021203 (2002).
[6] C. Mayer, V. Cabuil, T. Lalot, and R. Thouvenot, Adv. Mater. (Weinheim, Ger.) **12**, 417 (2000).
[7] S. Lecommandoux, O. Sandre, F. Chécot, J. Rodriguez-Hernandez, and R. Perzynski, Adv. Mater. (Weinheim, Ger.) **17**, 712 (2005).
[8] W. Wernsdorfer, E. B. Orozco, K. Hasselbach, A. Benoit, B. Barbara, N. Demoncy, A. Loiseau, H. Pascard, and D. Mailly, Phys. Rev. Lett. **78**, 1791 (1997).
[9] A. Roch, R. N. Muller, and P. Gillis, J. Chem. Phys. **110**, 5403 (1999).
[10] P. Trataj, M. del P. Morales, S. Veintemillas-Verdaguer, T. Gonzles-Carreo, and C. J. Serna, J. Phys. D **36**, R182 (2003).
[11] Yu. L. Raikher and R. Perzynski, in *Surface Effects in Magnetic Nanoparticles*, edited by D. Fiorani (Springer, New York, 2005).
[12] P. V. Hendriksen, S. Linderoth, and P-A. Lindgard, Phys. Rev. B **48**, 7259 (1993).
[13] P. V. Hendriksen, S. Linderoth, and P-A. Lingard, J. Magn. Magn. Mater. **104-107**, 1577 (1992).
[14] C. Caizer, J. Phys.: Condens. Matter **15**, 765 (2003).
[15] S. Linderoth, L. Balcells, A. Labarta, J. Tejada, P. V. Hendriksen, and S. A. Sethi, J. Magn. Magn. Mater. **124**, 269 (1993).
[16] J. P. Chen, C. M. Sorensen, K. J. Klabunde, G. C. Hadjipanayis, E. Devlin, and A. Kostikas, Phys. Rev. B **54**, 9288 (1996).
[17] F. Gazeau, E. Dubois, M. Hennion, R. Perzynski, and Yu. L. Raiker, Europhys. Lett. **40**, 575 (1997).
[18] B. Martinez, X. Obradors, Ll. Balcells, A. Rouanet, and C. Monty, Phys. Rev. Lett. **80**, 181 (1998).
[19] R. H. Kodama, A. E. Berkowitz, E. J. McNiff, and S. Foner, Phys. Rev. Lett. **77**, 394 (1996).
[20] J. M. D. Coey, Phys. Rev. Lett. **27**, 1140 (1971).
[21] P. Didukh, J. M. Greneche, A. Slawska-Waniewska, P. C. Fanin, and L. Casas, J. Magn. Magn. Mater. **242-245**, 613 (2002).
[22] H. Kachkachi, A. Ezzir, M. Nogues, and E. Tronc, Eur. Phys. J. B **14**, 681 (2000).
[23] E. Tronc, D. Fiorani, M. Nogues, A. M. Testa, F. Lucari, F. D'Orazio, J. M. Greneche, W. Wernsdorfer, N. Galvez, C. Chaneac, D. Mailly, and J. P. Jolivet, J. Magn. Magn. Mater. **262**, 6 (2003).
[24] E. De Biasi, C. A. Ramos, R. D. Zysler, and H. Romero, Phys. Rev. B **65**, 144416 (2002).
[25] F. A. Tourinho, R. Franck, and R. Massart, J. Mater. Sci. **25**, 3249 (1990).
[26] E. Dubois, V. Cabuil, F. Boue, and R. Perzynski, J. Chem. Phys. **111**, 7147 (1999).
[27] F. Cousin, E. Dubois, and V. Cabuil, Phys. Rev. E **68**, 021405 (2003).
[28] F. Gazeau, F. Boué, E. Dubois, and R. Perzynski, J. Phys.: Condens. Matter **15**, S1305 (2003).
[29] F. Gazeau, J. C. Bacri, F. Gendron, R. Perzynski, Yu. L. Raikher, V. Stepanov, and E. Dubois, J. Magn. Magn. Mater. **186**, 175 (1998).
[30] I. A. Campbell, H. Hurdequint, and F. Hippert, Phys. Rev. B **33**, 3540 (1986).
[31] M. H. Sousa, F. A. Tourinho, J. Depeyrot, G. J. da Silva, and M. C. F. L. Lara, J. Phys. Chem. B **105**, 1168 (2001).
[32] R. Aquino, F. A. Tourinho, R. Itri, M. C. F. L. Lara, and J. Depeyrot, J. Magn. Magn. Mater. **252**(1–3), 23 (2002).
[33] E. Tronc and D. Bonnin, J. Phys. (France) Lett. **46**, L437 (1985).
[34] P. V. Hendriksen, S. Linderoth, and P-A. Lingard, J. Phys.: Con-

dens. Matter **5**, 5675 (1993).
[35] C. R. Alves, M. H. Sousa, R. Aquino, H. R. Rechenberg, G. F. Goya, F. A. Tourinho, and J. Depeyrot, J. Metastable Nanocryst. Mater. **21**, 617 (2004).
[36] B. D. Cullity, *Introduction to Magnetic Materials* (Addison-Wesley, New York, 1972).
[37] L. del Bianco, A. Hernando, and D. Fiorani, Phys. Status Solidi A **189**, 533 (2002).
[38] T. Morita, J. Magn. Magn. Mater. **100**(1–3), 261 (1991).
[39] Yu. A. Koksharov, S. P. Gubin, I. D. Kosobudsky, G. Yu. Yurkov, D. A. Pankratov, L. A. Ponomarenko, M. G. Mikheev, M. Beltran, Y. Khodorkovsky, and A. M. Tishin, Phys. Rev. B **63**, 012407 (2000).
[40] A. J. Heeger and T. W. Houston, Phys. Rev. **135**, A661 (1964).
[41] J. L. Dormann, D. Fiorani, R. Cherkaoui, E. Tronc, F. Lucari, F. D'Orazio, L. Spinu, M. Nogues, H. Kachkachi, and J. P. Jolivet, J. Magn. Magn. Mater. **203**, 23 (1999).
[42] M. Garcia del Muro, X. Batlle, and A. Labarta, Phys. Rev. B **59**, 13584 (1999).